LETTERS

Structural basis for the coupling between activation and inactivation gates in K^+ channels

Luis G. Cuello[1]†, Vishwanath Jogini[1]†, D. Marien Cortes[1]†, Albert C. Pan[1]†, Dominique G. Gagnon[1], Olivier Dalmas[1], Julio F. Cordero-Morales[1], Sudha Chakrapani[1], Benoît Roux[1,2] & Eduardo Perozo[1,2]

The coupled interplay between activation and inactivation gating is a functional hallmark of K^+ channels[1,2]. This coupling has been experimentally demonstrated through ion interaction effects[3,4] and cysteine accessibility[1], and is associated with a well defined boundary of energetically coupled residues[2]. The structure of the K^+ channel KcsA in its fully open conformation, in addition to four other partial channel openings, richly illustrates the structural basis of activation–inactivation gating[5]. Here, we identify the mechanistic principles by which movements on the inner bundle gate trigger conformational changes at the selectivity filter, leading to the non-conductive C-type inactivated state. Analysis of a series of KcsA open structures suggests that, as a consequence of the hinge-bending and rotation of the TM2 helix, the aromatic ring of Phe 103 tilts towards residues Thr 74 and Thr 75 in the pore-helix and towards Ile 100 in the neighbouring subunit. This allows the network of hydrogen bonds among residues Trp 67, Glu 71 and Asp 80 to destabilize the selectivity filter[6,7], allowing entry to its non-conductive conformation. Mutations at position 103 have a size-dependent effect on gating kinetics: small side-chain substitutions F103A and F103C severely impair inactivation kinetics, whereas larger side chains such as F103W have more subtle effects. This suggests that the allosteric coupling between the inner helical bundle and the selectivity filter might rely on straightforward mechanical deformation propagated through a network of steric contacts. Average interactions calculated from molecular dynamics simulations show favourable open-state interaction-energies between Phe 103 and the surrounding residues. We probed similar interactions in the Shaker K^+ channel where inactivation was impaired in the mutant I470A. We propose that side-chain rearrangements at position 103 mechanically couple activation and inactivation in KcsA and a variety of other K^+ channels.

The K-channel pore-domain contains all the molecular elements necessary for ion conduction and for activation and inactivation gating[8,9]. Activation is classically associated with conformational rearrangements at the inner helix bundle[5,10–12], whereas C-type inactivation involves structural changes at the selectivity filter that alter its relationship with permeant ions[4,5,13–15]. Experimental demonstrations of the coupling between these two molecular 'gates' are based on the expectation that the conformation of one gate biases the conformational equilibrium of the other. High-affinity permeant ions such as Rb^+ and Cs^+, which interact intimately with the selectivity filter, slow the closure of the internal gate of many K^+ channels[4,16,17]. Mutations at or near the selectivity filter lead to a variety of gating effects in K^+ channels[11,18–20], whereas blocking by the amino-terminal inactivating particle, which tends to lock open the inner gate, greatly accelerates entry into the C-type inactivated state[3]. Experiments on the $K_{ir}1.1$ channel have shown that gating by either intracellular protons or extracellular K^+ ions appears to be coupled through conformational changes near the selectivity filter[21].

Taken together, these studies suggest that most K^+ channels open through coupled gates at both ends of the permeation path. Accordingly, a minimal kinetic cycle coupling these two dynamical elements[1,5,22] involves transitions between four states: closed inner gate with open-conductive filter (C/O); open inner gate with open-conductive filter (O/O); open inner gate with inactivated filter (O/I) and closed inner gate with inactivated filter (C/I). Observed kinetic behaviours can be described in terms of equilibrium population shifts among the four preexisting states:C/O, O/O, O/I and C/I. As in the concerted MWC model[23], opening of the inner gate (O/O $\leftrightarrow$ O/I) stabilizes the inactivated conformation of the filter, whereas transitioning into a C-type inactivated filter (O/I $\leftrightarrow$ C/I) biases the conformation of the inner gate towards the closed state (Supplementary Fig. 1).

In KcsA, cross-talk between the activation gate and the selectivity filter was first documented by electron paramagnetic resonance (EPR) spectroscopy on a limited set of residues in the pore-helix[12], where opening of the inner gate leads to subtle conformational changes in the pore-helix and outer vestibule (Supplementary Fig. 2). These conformational rearrangements, associated with C-type inactivation at the selectivity filter[6,7], are also coupled to the opening of the activation gate[24]. An accompanying paper[5] suggests a molecular mechanism for C-type inactivation from the crystal structure of the O/I state and a series of partially O/I structures. Using these structures as a baseline, we have examined the mechanistic principles underlying the conformational coupling between activation and inactivation gates in KcsA.

We first estimated the degree of allosteric coupling between proton-dependent activation and C-type inactivation through bi-directional perturbation in each of the gates. We monitored the conformation of the inner bundle gate by EPR spectroscopy while influencing the stability of the conductive conformation of the selectivity filter in two different ways: by inhibiting C-type inactivation through the E71A mutant and by slowing down entry into C-type inactivation in the presence of Rb^+ ions. In both cases, the pH dependence of the inner bundle gate conformation shifts towards lower proton concentrations (Fig. 1a). We also found this effect when the channels were bathed in Cs^+, but not in the presence of impermeant ions (Supplementary Fig. 3). As the selectivity filter inactivates mostly from the open state[24], we interpret these shifts as the energetic cost paid by the activation gate to favour the collapse of the selectivity filter. Stabilizing the conductive conformation of the filter therefore reduces the amount of energy required to open the inner gate. The structure of

[1]Department of Biochemistry and Molecular Biology, The University of Chicago, 929 E 57th Street, Chicago, Illinois 60637, USA. [2]Institute for Biophysical Dynamics, The University of Chicago, 929 E 57th Street, Chicago, Illinois 60637, USA. †Present address: Department of Cell Physiology and Molecular Biophysics, Texas Tech University, Lubbock, Texas 79430, USA (L.G.C, D.M.C.); D. E. Shaw Research, Hyderabad 500034, India (V.J.); D. E. Shaw Research, New York, New York 10036, USA (A.C.P.).

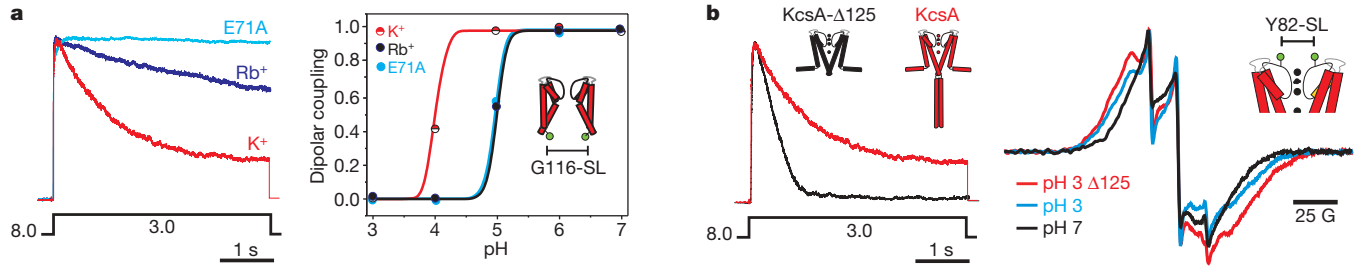

Figure 1 | Conformational coupling between activation and inactivation gates in K^+ channels. **a**, Defining coupling from the selectivity filter to the activation gate by modulating the rate and extent of inactivation. Left panel, KcsA macroscopic currents obtained at 100 mV from liposome-reconstituted KcsA in 100 mM symmetric KCl (red), 100 mM symmetric RbCl (navy blue) and the mutant E71A in 100 mM symmetric KCl (light blue). Right panel, extent of inner-gate opening for these three conditions in KcsA spin-labelled at G116C and monitored from the amplitude of the central resonance line normalized by the total number of spins. Red, asolectin-reconstituted spin-labelled (SL) channels in 100 mM symmetric KCl; navy blue, in 100 mM symmetric ; light blue, the mutant E71A in 100 mM symmetric KCl. **b**, Defining coupling from the activation gate to the selectivity filter by modulating the extent of inner-gate opening. Left panel, macroscopic currents at 100 mV and 100 mM symmetric KCl for wild-type (WT) KcsA (red) and chymotrypsin C-terminal-truncated channel KcsA-Δ125 (black). Right panel, EPR spectra from the spin labelled Y82C mutant in the closed, conductive state (pH 7, black), open, inactivated state (pH 3, blue) and the C-terminal truncated open, inactivated state (pH 3, red). EPR spectra were normalized by the total number of spins in the sample.

a fully open KcsA (32 Å diameter opening) in the presence of Rb^+ ions (3.3 Å resolution) consistently shows that the filter cannot fully enter the collapsed inactivated state; compare to the K^+-occupied pore (Supplementary Fig. 4).

If gate-coupling is indeed bidirectional, a perturbation at the activation gate should also modify the energetic stability of the selectivity filter. Figure 1b shows that deletion of the channel carboxy-terminal helix bundle (KcsA-Δ125) sharply increases the rate and extent of inactivation without major effects on activation kinetics, leading to very low open probabilities at steady state. Accordingly, truncation of the channel C-terminal domain leads to increased gate opening (Supplementary Fig. 5) and a subtle increase in dipolar coupling (increased proximity) between spin labels at position Tyr 82 (ref. 12) (Fig. 1b, right panel) consistent with the proposed 'collapsing' or 'pinching' of the selectivity filter[25].

Evaluation of a series of KcsA structures with various degrees of gate opening[5] suggests a likely mechanism underlying the transition from the C/O state to the O/I state. A sequential analysis of these crystal structures (Fig. 2a, Supplementary Fig. 6) revealed step-wise conformational changes at Phe 103, a residue close to the C-terminal end of the KcsA pore-helix. Phe 103 changes its rotameric conformation as a function of channel-opening (Fig. 2b–d) so that, given its spatial proximity to the selectivity filter, a steric clash could in principle promote the collapse of the filter. In fact, the side chain of Phe 103 is energetically obligated to change its rotameric state in response to the conformational change of the inner helix associated with the opening of the intracellular activation gate (Supplementary Fig. 7). Additional pieces of information provide some clues to the mode of action of Phe 103 and how it affects the stability of the conductive state of the selectivity filter.

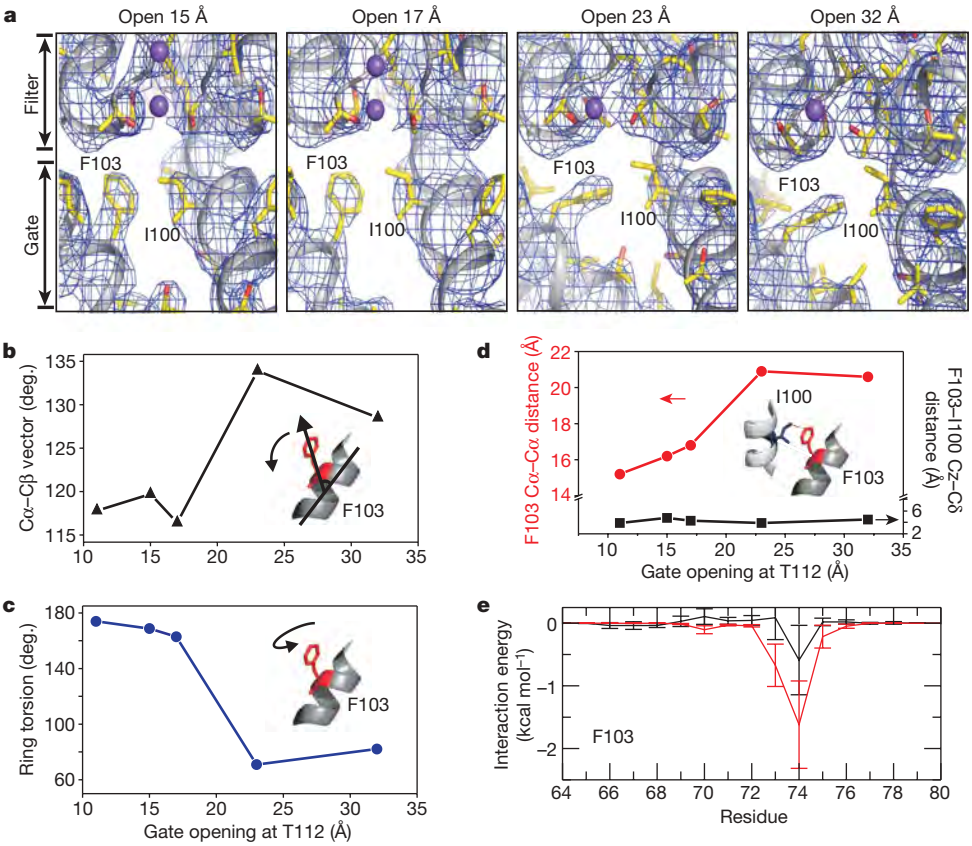

Figure 2 | Structural basis for allosteric coupling in KcsA. **a**, Conformational rearrangements in the KcsA aqueous cavity in a series of partially opened structures[5]. The composite omit map (contoured at 2σ) of the channel corresponding to two neighbouring subunits is shown as a blue mesh. Transmembrane helices are represented as ribbons, residues Ile 100 and Phe 103 are shown in stick representation, and ions are shown as space-filling spheres. **b**, Dependence of the Phe 103 side-chain tilting with the degree of opening of the inner bundle gate at Thr 112. **c**, Dependence of torsional angle on the degree of opening. **d**, Variation with the degree of opening of Cα–Cα inter-subunit distance (red) and distance between Phe 103 and Ile 100 from adjacent subunits (black). **e**, Interaction energies of residue Phe 103 in TM2 with individual side chains from residues in the pore-helix.

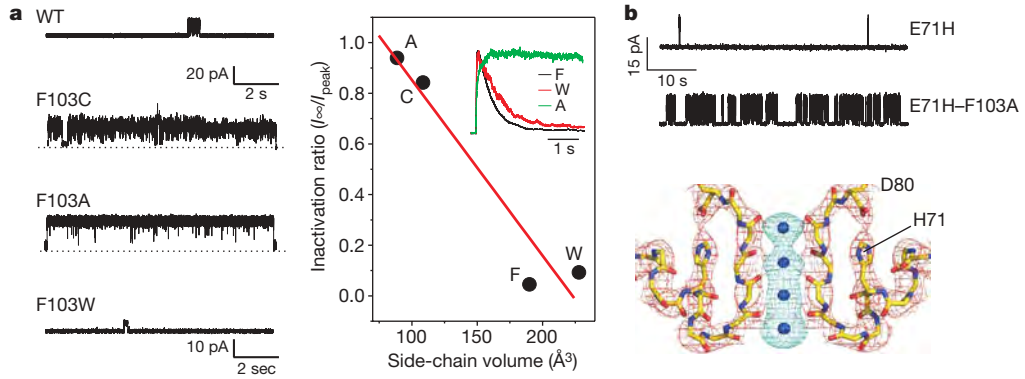

Figure 3 | Role of Phe 103 in allosteric coupling with the selectivity filter. **a**, The mutation F103A sharply reduces the rate and extent of C-type inactivation. Left panel, representative single-channel recordings from asolectin-reconstituted channels in symmetric 200 mM KCl. Right panel, the extent of steady-state inactivation from the ratio between peak (I_{peak}) and steady state (I_{∞}) current, plotted as a function of side-chain volume for four substitutions at position 103. Multiple side-chain substitutions at position 103 show a volume-dependence of the extent of inactivation, as derived from macroscopic currents during pH pulse experiments (inset). **b**, Mutation of Phe 103 disrupts C-type inactivation in the deeply inactivated mutant E71H. Top panel, representative single-channel recordings in symmetric 100 mM KCl from the E71H mutant background and the E71H–F103A double-mutant. Bottom panel, crystal structure of E71H–F103A KcsA, determined at 3 Å resolution. Shown are the $2F_o$–F_c electron density map (pink mesh contoured at 2σ) of the filter corresponding to residues 70–80 from two diagonally symmetric subunits and the F_o–F_c omit map (blue mesh contoured at 3σ) corresponding to ions in the filter.

EPR spectroscopy indicates that when KcsA undergoes activation-gating, the steric contacts of a spin-label attached to the mutant F103C increase (Supplementary Fig. 8). Furthermore, we have shown that the activation gate appears to compress the first helical turn (C-terminal end) of the pore-helix when maximally open, leading to the helical pitch shortening slightly[5]. These observations suggest that the allosteric coupling with the selectivity filter is steric in nature. To probe the molecular origin of the coupling between the activation gate and the selectivity filter, we examined the average interactions between the aromatic ring of Phe 103 and residues along the pore-helix during a molecular dynamics simulation. We found significant non-polar van der Waals interactions (-2.4 kcal mol^{-1}) between the Phe 103 side chain and Ile 100 in the neighbouring subunit and between Phe 103 and Thr 74/Thr 75 in the same subunit, with additional minor interactions of Phe 103 with Met 96 (Fig. 2e). These observations are consistent with solid-state NMR chemical-shift mapping that suggests a role for the interaction between Ile 100 and residues Thr 72–Thr 75 in activation–inactivation coupling[26]; they help to explain the intrinsic cooperativity of the process[27].

These calculations implicitly predict that severing the integrity of the coupling element should stop communication between the two gates, generating a non-inactivating channel. Figure 3 shows that this is indeed the case. Mutating Phe 103 to alanine inhibits entry into the inactivated conformation, as shown by steady-state single channel (Fig. 3a, left) and macroscopic (Fig. 3a, right, inset) currents at +100 mV. Further, interaction energies are sharply decreased in F103A (Supplementary Fig. 9). Mutations at position 103 seemed to influence C-type inactivation in a size-dependent way: small side-chain substitutions F103A and F103C limited entry into the inactivated state, whereas the larger F103W allowed the channel to inactivate (Fig. 3a).

The role of Phe 103 in the allosteric communication between activation and inactivation gates is further supported by introduction of the mutation F103A on the background of the extremely inactivating mutant E71H[7]. E71H readily enters the inactivated state by strengthening the interaction with Asp 80 at the top of the selectivity filter, even in the closed or partially open states, leading to very short mean open times and a low steady-state open probability[7]. In single-channel traces, substitution of the Phe 103 by an alanine on the E71H frame greatly destabilizes the inactivated conformation, increasing both mean open times and steady-state open probability (Fig. 3b, top panel). In agreement with this, the crystal structure of E71H–F103A KcsA, determined at 3 Å resolution (Fig. 3b, bottom), shows the conductive form of the selectivity filter with its full complement of K^+ ions, similar to that observed in closed KcsA.

Given the high degree of functional and structural conservation among K^+ channel pore-domains, it is tempting to suggest that a common structural motif mediates the communication between gates in the K^+ channel superfamily. To assess whether the information

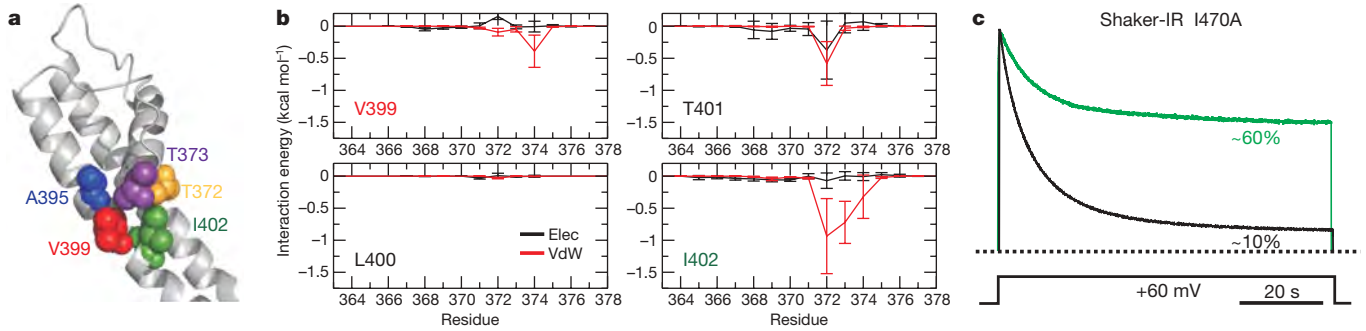

Figure 4 | A common gate-coupling mechanism in K^+ channels. **a**, Structural representation of the interface between the inner bundle gate (S6) and the pore-helix in the $K_v1.2$ pore-domain (2R9R) with key amino acid side chains shown as van der Waals spheres (equivalent KcsA/$K_v1.2$ positions: Met 96/Ala 391, blue; Ile 100/Val 399, red; Phe 103/Ile 402, green; Thr 74/Thr 373, yellow; Thr 75/Thr 374, purple). **b**, Interaction energies of selected $K_v1.2$ residues in TM2 (equivalent to those in KcsA) with individual side chains from residues in the pore-helix. Elec, electrostatic interactions; VdW, van der Waals interactions. Error bars, mean ± s.d. **c**, Equivalent role of Ile 470 in gate-coupling in Shaker. Representative cut-open oocyte voltage-clamp traces obtained from N-type inactivation-removed Shaker (Shaker-IR) (black) and the mutation I470A (green) expressed in *Xenopus* oocytes ($n = 5$ for I470A). Currents were normalized to the peak current.

flowing between the two gates in a K_v channel follows the same pathway as in KcsA, we evaluated the role of the residues equivalent to Phe 103: a position which is often occupied by a bulky isoleucine (Supplementary Fig. 10). Interaction-energy calculations for Ile 402 in the $K_v1.2$ channel suggest strong van der Waals coupling with Thr 372 and Thr 373 (equivalent to Thr 74 and Thr 75 in KcsA) in the pore-helix of the same subunit as seen in KcsA (Fig. 4b). Mutating the same position in the pore domain of Shaker K_v channel (Ile 470) to alanine effectively destabilizes the C-type inactivated state as determined from cut-open oocyte voltage-clamp experiments (Fig. 4c). This is in agreement with the effect of mutant I470C in Shaker[28], which severely reduced the rate of C-type inactivation, and with the role of the analogous position on human ERG (Tyr 652) channels in inactivation gating[29]. When we mutated residue Ile 470 to a tyrosine in Shaker an inverted inactivating phenotype was observed, reminiscent of the fast inactivation of human ERG channels[30].

The basic features of the network of residues forming this allosteric communication pathway seem to be conserved from prokaryotes to eukaryotes. Key among these residues is Phe 103 in KcsA and its equivalent position in K_v channels. Although the nature of the interactions between Phe 103 and the pore-helix is yet to be explained, the apparent volume-dependence in C-type inactivation coupling suggests that a steric component has a significant role. More importantly, the present mechanism can lend a structural basis to the complex interplay between C-type inactivation and pore-block in hERG channels, with obvious clinical relevance[29].

METHODS SUMMARY

We performed single-channel and macroscopic current measurements by liposome patch-clamping, as described[7]. We evaluated the conformational state of the inner bundle gate by continuous wave-EPR and fluorescence spectroscopy. We performed site-directed spin and fluorophore labelling were position G116 before reconstituting the channel onto pre-formed asolectin liposomes. We obtained crystals of the E71H–F103A mutant and of the open KcsA mutant in Rb^+ ions in complex with a Fab fragment by the sitting drop method in 20–25% polyethylene glycol (PEG) 400 (v/v), 50 mM magnesium acetate, 50 mM sodium acetate (pH 5.4–5.6) at 20 °C. We determined the structures by molecular replacement of the Fab fragment and the extracellular part of wild-type (WT) KcsA (Protein Data Bank (PDB) 1K4C) without the selectivity filter as search model. We performed molecular dynamics simulations with an all-atom system that included the open inactive KcsA channel[7] embedded in dipalmitoylphosphatidylcholine (DPPC) lipids and surrounded by an aqueous solution of 200 mM KCl. Average interaction energies were calculated from molecular dynamics simulations performed using the programs CHARMM and NAMD with the all-atom PARAM27 force field.

Full Methods and any associated references are available in the online version of the paper at www.nature.com/nature.

Received 8 October 2009; accepted 30 April 2010.

1. Panyi, G. & Deutsch, C. Cross talk between activation and slow inactivation gates of Shaker potassium channels. *J. Gen. Physiol.* **128,** 547–559 (2006).
2. Sadovsky, E. & Yifrach, O. Principles underlying energetic coupling along an allosteric communication trajectory of a voltage-activated K^+ channel. *Proc. Natl Acad. Sci. USA* **104,** 19813–19818 (2007).
3. Baukrowitz, T. & Yellen, G. Use-dependent blockers and exit rate of the last ion from the multi-ion pore of a K^+ channel. *Science* **271,** 653–656 (1996).
4. Lopez-Barneo, J., Hoshi, T., Heinemann, S. H. & Aldrich, R. W. Effects of external cations and mutations in the pore region on C-type inactivation of Shaker potassium channels. *Receptors Channels* **1,** 61–71 (1993).
5. Cuello, L., Jogini, V. & Perozo, E. Structural mechanism of C-type inactivation in K^+ channnels. *Nature* doi:10.1038/nature09153 (this issue) (2010).
6. Cordero-Morales, J. F. *et al.* Molecular determinants of gating at the potassium-channel selectivity filter. *Nature Struct. Mol. Biol.* **13,** 311–318 (2006).
7. Cordero-Morales, J. F. *et al.* Molecular driving forces determining potassium channel slow inactivation. *Nature Struct. Mol. Biol.* **14,** 1062–1069 (2007).
8. Armstrong, C. M. Voltage-gated K channels. *Sci. STKE* **2003,** re10 (2003).
9. Yellen, G. The voltage-gated potassium channels and their relatives. *Nature* **419,** 35–42 (2002).
10. Jiang, Y. *et al.* Crystal structure and mechanism of a calcium-gated potassium channel. *Nature* **417,** 515–522 (2002).
11. Liu, Y., Holmgren, M., Jurman, M. E. & Yellen, G. Gated access to the pore of a voltage-dependent K^+ channel. *Neuron* **19,** 175–184 (1997).
12. Perozo, E., Cortes, D. M. & Cuello, L. G. Structural rearrangements underlying K^+-channel activation gating. *Science* **285,** 73–78 (1999).
13. Choi, K. L., Aldrich, R. W. & Yellen, G. Tetraethylammonium blockade distinguishes two inactivation mechanisms in voltage-activated K^+ channels. *Proc. Natl Acad. Sci. USA* **88,** 5092–5095 (1991).
14. Hoshi, T., Zagotta, W. N. & Aldrich, R. W. Biophysical and molecular mechanisms of Shaker potassium channel inactivation. *Science* **250,** 533–538 (1990).
15. Kiss, L., LoTurco, J. & Korn, S. J. Contribution of the selectivity filter to inactivation in potassium channels. *Biophys. J.* **76,** 253–263 (1999).
16. Demo, S. D. & Yellen, G. Ion effects on gating of the Ca^{2+}-activated K^+ channel correlate with occupancy of the pore. *Biophys. J.* **61,** 639–648 (1992).
17. Swenson, R. P. Jr & Armstrong, C. M. K^+ channels close more slowly in the presence of external K^+ and Rb^+. *Nature* **291,** 427–429 (1981).
18. Alagem, N., Yesylevskyy, S. & Reuveny, E. The pore helix is involved in stabilizing the open state of inwardly rectifying K^+ channels. *Biophys. J.* **85,** 300–312 (2003).
19. Chapman, M. L., Blanke, M. L., Krovetz, H. S. & Vandongen, A. M. Allosteric effects of external K^+ ions mediated by the aspartate of the GYGD signature sequence in the Kv2.1 K^+ channel. *Pflügers Arch.* **451,** 776–792 (2006).
20. Proks, P., Capener, C. E., Jones, P. & Ashcroft, F. M. Mutations within the P-loop of Kir6.2 modulate the intraburst kinetics of the ATP-sensitive potassium channel. *J. Gen. Physiol.* **118,** 341–353 (2001).
21. Schulte, U., Weidemann, S., Ludwig, J., Ruppersberg, J. & Fakler, B. K^+-dependent gating of $K_{ir}1.1$ channels is linked to pH gating through a conformational change in the pore. *J. Physiol. (Lond.)* **534,** 49–58 (2001).
22. Ben-Abu, Y., Zhou, Y., Zilberberg, N. & Yifrach, O. Inverse coupling in leak and voltage-activated K^+ channel gates underlies distinct roles in electrical signaling. *Nature Struct. Mol. Biol.* **16,** 71–79 (2009).
23. Monod, J., Wyman, J. & Changeux, J. P. On the nature of allosteric transitions: a plausible model. *J. Mol. Biol.* **12,** 88–118 (1965).
24. Chakrapani, S., Cordero-Morales, J. F. & Perozo, E. A quantitative description of KcsA gating I: macroscopic currents. *J. Gen. Physiol.* **130,** 465–478 (2007).
25. Liu, Y., Jurman, M. E. & Yellen, G. Dynamic rearrangement of the outer mouth of a K^+ channel during gating. *Neuron* **16,** 859–867 (1996).
26. Ader, C. *et al.* Coupling of activation and inactivation gate in a K^+-channel: potassium and ligand sensitivity. *EMBO J.* **28,** 2825–2834 (2009).
27. Rotem, D., Mason, A. & Bayley, H. Inactivation of the KcsA potassium channel explored with heterotetramers. *J. Gen. Physiol.* **135,** 29–42 (2010).
28. Olcese, R., Sigg, D., Latorre, R., Bezanilla, F. & Stefani, E. A conducting state with properties of a slow inactivated state in a Shaker K^+ channel mutant. *J. Gen. Physiol.* **117,** 149–163 (2001).
29. Chen, J., Seebohm, G. & Sanguinetti, M. C. Position of aromatic residues in the S6 domain, not inactivation, dictates cisapride sensitivity of HERG and eag potassium channels. *Proc. Natl Acad. Sci. USA* **99,** 12461–12466 (2002).
30. Klement, G., Nilsson, J., Arhem, P. & Elinder, F. A tyrosine substitution in the cavity wall of a K channel induces an inverted inactivation. *Biophys. J.* **94,** 3014–3022 (2008).

Supplementary Information is linked to the online version of the paper at www.nature.com/nature.

Acknowledgements We thank F. Bezanilla, H Mchaourab and R. Nakamoto for discussions and comments on the manuscript. We also thank K. Locher for comments on the manuscript. R. Mackinnon provided the Fab-expressing hybridoma cells. We thank the members of the Perozo laboratory for comments on the manuscript. We thank K. R. Rajashankar, R. Sanishvili and the staff at the NE-CAT 24ID and GM-CA 23ID beamlines at the Advanced Photon Source, Argonne National Laboratory for assistance during data collection. This work was supported in part by NIH grant R01-GM57846 and a gift from the Palmer family to E.P., by grant R01-GM62342 to B.R. and by an NRSA postdoctoral fellowship to A.C.P.

Author Contributions E.P. and L.G.C. conceived the project. L.G.C. and D.M.C. generated constructs, performed biochemical analysis, and expressed, purified and crystallized the proteins. L.G.C. performed EPR experiments. L.G.C., V.J. and E.P. collected X-ray diffraction data. L.G.C. and V.J. determined and analysed the structures. A.C.P. and B.R. performed computation analysis. O.D. and L.G.C. conducted FRET measurements. S.C. measured inactivation in truncated KcsA and in Rb^+ ions. J.F.C.-M. measured E71H single-channel activity and made the F103A mutation. L.G.C. measured F103X mutant series electrophysiology. D.G.G. made electrophysiology measurements in Shaker channels. E.P., L.G.C. and V.J. analysed the data and wrote the paper.

Author Information The atomic coordinates of the mutant E71H–F103A in the KcsA–OM background and of KcsA–OM in Rb^+ ions have been deposited in the Protein Data Bank under accession codes 3HPL and 3FB7, respectively. Reprints and permissions information is available at www.nature.com/reprints. The authors declare no competing financial interests. Readers are welcome to comment on the online version of this article at www.nature.com/nature. Correspondence and requests for materials should be addressed to E.P. (eperozo@uchcicago.edu).

METHODS

Molecular biology and protein expression. We used the PCR-overlapping method to introduce all mutations at once when generating the open mutant KcsA (KcsA–OM) constructs. We expressed and purified KcsA–OM as described[31,32], with some modifications. We performed protein expression in *Escherichia coli* at 30 °C and 20 mM $BaCl_2$ for 18 h. We purified proteins purification by solubilizing KcsA-containing *E. coli* membranes with 10 mM dodecylmaltoside (ANATRACE) in a buffer with 150 mM KCl and 50 mM Tris-Cl pH 7.0. We centrifuged the solubilization mixture at 100,000*g*, loaded the supernatant onto a cobalt column (TALON) and washed extensively with 10 mM imidazole followed by elution with 500 mM imidazole. After purification, we loaded the protein onto a Superdex HR 200 (Amersham) size-exclusion chromatographic column to assess proper folding and stability of KcsA.

Spin-labelling of cysteine mutants for EPR and reconstitution in liposomes. While they were still bound to the cobalt column, we washed KcsA cysteine mutants extensively with 0.5 mM TCEP/TCYP reducing agent and eluted them with previously degassed buffer. Once the protein was eluted, we concentrated it to 3–4 mg ml^{-1} and labelled it with methane-thiosulphonate spin-label (MTS-SL; Toronto Research Chemical) in a 10:1 SL-to-channel molar ratio. We removed excess spin label before reconstitution by passing the mixture through a desalting column (PD-10 column, AMERSHAM). We reconstituted KcsA spin-labelled mutant in preformed asolectin liposome in a 1:400 channel-to-lipid molar ratio. After diluting the protein-liposome mixture with a buffer containing 150 mM KCl and 50 mM Tris-Cl pH 7.0, we incubated the sample overnight with ~0.5 g Bio-Beads (Bio-Rad). We centrifuged the samples at 100,000*g* for 2 h. To elicit pH-dependent conformational changes, we resuspended the samples with a high-capacity buffer at the desired pH and/or ionic strength and then spun them down to a small pellet, which we resuspended in a small volume for EPR measurements[12,33,34].

Fluorescence spectroscopy. We labelled Purified KcsA–OM 116C with a tenfold molar excess of a mixture of Alexa-Fluor350 (donor) and Alexa-Fluor 488 (acceptor), where the proportion of acceptor varies from 0 to 1. After 2 h we stopped the labelling reactions by adding a large excess of L-cysteine, and removed the excess of probe using a PD10 desalting column (Amersham), followed by gel exclusion chromatography on an Amersham Sephadex 200 FPLC. We split each of the labelled samples into two fractions, submitting one of them to chymotrypsin digestion as previously described. We then normalized the truncated and non-truncated samples to the same donor concentration and recorded the fluorescence spectra ($\lambda_{ex} = 350$ nm) on a steady-state photon-counting fluorimeter (QM-4 PTI) from 400 to 650 nm. We plotted the normalized fluorescence intensity (F_{DA}/F_D) as a function of the acceptor molar fraction a, and fitted the experimental plot with the equation $I_{DA}/I_D = 1 - E + E(1 - a)^{n-1}$, where E is the transfer efficiency and n the oligomeric state. Our experimental results were best fitted when $n = 4$ (tetramer).

Liposome patch-clamp. We patch-clamped liposome-reconstituted KcsA following the method of ref. 35, with some modifications[6,36]. We reconstituted KcsA as above at protein-to-lipid ratios varying from 1:100 to 1:5,000. We centrifuged the proteoliposome suspension for 1 h at 100,000*g*, and resuspended the pellet, corresponding to 10 mg of lipids in 60 µl of rehydration buffer. Typically, we dried three drops of the overnight in a desiccation chamber under vacuum for 24 h, at which time we applied 20 µl of rehydration buffer to each dried drop. We allowed rehydration to proceed for 5 h, yielding liposomes suitable for patch-clamp. Except where indicated, we took all patch-clamp measurements in symmetrical conditions: 200 mM KCl and MOPS buffer, pH 4.0, at room temperature (23 °C). We recorded single-channel currents with an Axopatch 200B patch-clamp amplifier, and sampled currents at 40 kHz with analogue filter set to 2 kHz (−3 dB). Pipette resistances were 2 MΩ.

Crystallization of KcsA–OM. We expressed and purified mutant E71H–F103A in the KcsA background to homogeneity as described above. We crystallized the channel in the presence of antibody Fab fragment by the sitting-drop method as described previously[37]. For crystals of KcsA–OM with Rb^+, we exchanged K^+ for 150 mM RbCl by gel filtration after complex formation. Cubic crystals of KcsA–Fab complex appeared after a week in a sitting-drop with the following composition: 20–25% PEG400 (v/v), 50 mM magnesium acetate, 50 mM sodium acetate (pH 5.4–6.0) at 23 °C. Based on our previous experience, we regularly increased PEG concentration in the reservoir to decrease the water content in the drop, to achieve reduced B-factors. Crystals diffracted to Bragg spacing of 3.3 Å. We collected data on beamlines 23-ID (GM/CA-CAT) and 24-ID-C (NE-CAT) at the Advanced Photon Source and processed it with the HKL2000 package[38].

Crystallographic analysis. We solved structures by molecular replacement, using only the Fab fragment and the extracellular part of WT KcsA (PDB 1K4C) without the selectivity filter as a search model to reduce the biasing of model prediction, because the expected conformation is supposed to be different from the closed state. In the first cycle of refinement using CNS software[39], the electron-density that appeared corresponded to the intracellular part with TM2 splayed; this electron density was filled by manual rebuilding using the O program[40]. We built the selectivity filter with side-chain density corresponding to V76, Y78 and D80 as markers. We performed several cycles of manual rebuilding and refinement until we had built the complete model into the electron-density while minimizing R factor values. We could see electron-density up to only residue 117 in open-inactivated and 112 in open-activated structures; unresolved side chains were assigned as alanines. For data collection and refinement statistics, see Supplementary Table 1. We obtained one-dimensional electron-density profiles along the symmetry axis of the selectivity filter for structures in Rb^+ as described elsewhere. We used CNS[37,41] to calculate the difference Fourier maps of the open-activated structure at 3.3 Å and the closed-state structure (PDB 1R3I) at 2.4 Å in the presence of Rb^+. We did not scale down the resolution of the closed state because we are interested in qualitative comparison of the electron-density peaks corresponding to the ions in the filter-binding sites.

Molecular dynamics simulations. To represent the simulation system, we used an atomic model of the open-inactive KcsA channel[5] embedded in DPPC lipids and surrounded by an aqueous solution of 150 mM KCl. The model contained the KcsA tetramer (404 amino acid residues), 112 DPPC molecules, 7,325 water molecules and 2 K^+ ions in the pore at positions S1 and S4. To ensure electrical neutrality and mimic a 150 mM KCl concentration, we added 18 K^+ and 32 Cl^- ions to the bulk solution. We set up the system using the CHARMM program[42] following a previously described methodology[43]. We used the NAMD program[44] for constant-pressure molecular dynamics simulations. We generated the F103A mutation system *in silico* on all four KcsA subunits and carefully equilibrated it before the production run. We calculated interaction energies between the side chain of residue 103 with residues 60 to 80 on the same subunit averaged over all four subunits during an 11.5-ns molecular dynamics trajectory. The $K_v1.2$ simulations were described previously[45]. Error bars are standard deviations over interaction-energy averages sampled once every picosecond. We obtained adiabatic energy maps by varying the χ_1 and χ_2 dihedral angles of Phe 103 in one subunit of KcsA and calculating the energy of those conformations after performing a minimization. The system consisted of the KcsA tetramer in vacuum. Atoms far from the Phe 103 were fixed in space (residues 22 to 28, 46 to 65 and 115 to 124) and heavy atoms near Phe 103 (all others except for the Phe 103 side chain) were harmonically restrained with a force-constant of 100 kcal mol^{-1} $Å^{-2}$).

31. Cuello, L. G., Romero, J. G., Cortes, D. M. & Perozo, E. pH-dependent gating in the *Streptomyces lividans* K^+ channel. *Biochemistry* **37,** 3229–3236 (1998).
32. Cortes, D. M. & Perozo, E. Structural dynamics of the *Streptomyces lividans* K^+ channel (SKC1): oligomeric stoichiometry and stability. *Biochemistry* **36,** 10343–10352 (1997).
33. Liu, Y. S., Sompornpisut, P. & Perozo, E. Structure of the KcsA channel intracellular gate in the open state. *Nature Struct. Biol.* **8,** 883–887 (2001).
34. Cuello, L. G., Cortes, D. M. & Perozo, E. Molecular architecture of the KvAP voltage-dependent K^+ channel in a lipid bilayer. *Science* **306,** 491–495 (2004).
35. Delcour, A. H., Martinac, B., Adler, J. & Kung, C. Modified reconstitution method used in patch-clamp studies of *Escherichia coli* ion channels. *Biophys. J.* **56,** 631–636 (1989).
36. Cortes, D. M., Cuello, L. G. & Perozo, E. Molecular architecture of full-length KcsA: role of cytoplasmic domains in ion permeation and activation gating. *J. Gen. Physiol.* **117,** 165–180 (2001).
37. Zhou, Y., Morais-Cabral, J. H., Kaufman, A. & MacKinnon, R. Chemistry of ion coordination and hydration revealed by a K^+ channel-Fab complex at 2.0 Å resolution. *Nature* **414,** 43–48 (2001).
38. Otwinowski, Z., &. Minor, W. Processing of X-ray diffraction data collected in oscillation mode. *Methods Enzymol.* **276,** 307–332 (1997).
39. Brünger, A. T. *et al.* Crystallography & NMR system: A new software suite for macromolecular structure determination. *Acta Crystallogr. D* **54,** 905–921 (1998).
40. Jones, T. A., Zou, J. Y., Cowan, S. W. & Kjeldgaard, M. Improved methods for building protein models in electron density maps and the location of errors in these models. *Acta Crystallogr. A* **47,** 110–119 (1991).
41. Morais-Cabral, J. H., Zhou, Y. & MacKinnon, R. Energetic optimization of ion conduction rate by the K^+ selectivity filter. *Nature* **414,** 37–42 (2001).
42. Brooks, B. R. *et al.* CHARMM: a program for macromolecular energy, minimization, and dynamics calculations. *J. Comput. Chem.* **4,** 187–217 (1983).
43. Bernèche, S. & Roux, B. Molecular dynamics of the KcsA K^+ channel in a bilayer membrane. *Biophys. J.* **78,** 2900–2917 (2000).
44. Phillips, J. C. *et al.* Scalable molecular dynamics with NAMD. *J. Comput. Chem.* **26,** 1781–1802 (2005).
45. Jogini, V. & Roux, B. Dynamics of the Kv1.2 voltage-gated K^+ channel in a membrane environment. *Biophys. J.* **93,** 3070–3082 (2007).